

Geometric measure of entanglement from Wehrl Moments using Artificial Neural Networks

Jérôme Denis, François Damanet and John Martin[†]

Institut de Physique Nucléaire, Atomique et de Spectroscopie, CESAM, University of Liège,
B-4000 Liège, Belgium

[†] jmartin@uliege.be

May 30, 2022

Abstract

In recent years, artificial neural networks (ANNs) have become an increasingly popular tool for studying problems in quantum theory, and in particular entanglement theory. In this work, we analyse to what extent ANNs can provide us with an accurate estimate of the geometric measure of entanglement of symmetric multiqubit states on the basis of a few Wehrl moments (moments of the Husimi function of the state). We compare the results we obtain by training ANNs with the informed use of convergence acceleration methods. We find that even some of the most powerful convergence acceleration algorithms do not compete with ANNs when given the same input data, provided that enough data is available to train these ANNs. More generally, this work opens up perspectives for the estimation of entanglement measures and other $SU(2)$ invariant quantities, such as Wehrl entropy, on the basis of a few Wehrl moments that should be more easily accessible in experiments than full state tomography.

Contents

1	Introduction	2
2	Wehrl moments and geometric measure of entanglement	3
2.1	Multiqubit symmetric states	3
2.2	Husimi function and Wehrl moments	4
2.2.1	Husimi function	4
2.2.2	Wehrl moments – explicit expressions	4
2.3	Geometric measure of entanglement	5
2.4	Bounds on GME from Wehrl moments	5
3	Datasets and performance metrics	7
3.1	Generation of datasets	7
3.2	Performance metrics	8
4	Estimation of the geometric measure of entanglement	8
4.1	Wehrl moments ratios	9
4.2	Convergence acceleration algorithms	9

4.3	Artificial Neural Networks	11
5	Discussion	12
6	Conclusion	13
A	Explicit expression of Wehrl moments in terms of $ \epsilon_i\rangle$	14
B	Asymptotic behaviour of the Wehrl moments	16
C	Additional information on ANNs	17
	References	18

1 Introduction

Entanglement is at the heart of quantum physics and constitutes a crucial resource for most quantum technologies [1]. Estimating the entanglement of a system is usually a challenging task, both theoretically and experimentally, and the development of theoretical methods and experimental protocols are essential in this context.

Here we tackle the problem of estimating entanglement via the use of artificial neural networks (ANNs). Over the past few years, deep learning methods have gained momentum in quantum physics [2, 3]. In the context of quantum state tomography, they have been used to reconstruct density matrices from measurement results [4, 5] and to find an optimal measurement basis [6]. In quantum optics, artificial neural networks have been trained to detect multimode Wigner negativity [7]. Deep reinforcement learning and recurrent neural networks have also been exploited for quantum information theory purposes, such as quantum state preparation [8] and quantum error-correction [9, 10].

In the context of entanglement theory, ANNs have been used to quantify the amount of entanglement in multipartite quantum systems [11, 12] and to classify the entanglement in pure states [13] and mixed states [14]. In [11], the authors trained complex-valued ANNs to predict the geometric measure of entanglement (GME) of symmetric states. To do so, they reformulated the GME computational problem as the search for the best rank-one tensor approximation of complex tensors, for which they used ANNs. Other authors have used deep learning methods to compute the concurrence and mutual information from an incomplete tomography of mixed qubit states [12]. In quantum many-body physics, convolutional neural networks were employed to compute e.g. the entanglement entropy from the variance on the number of particles in an electron chain [15].

More specifically, the general question posed in this work, which is along these lines, is: *To what extent can the geometric measure of entanglement of symmetric multiqubit states be estimated on the basis of partial information in the form of some of their Wehrl moments?* Wehrl moments are the moments of the Husimi Q function of a state [16]. They have been used to define measures of non-classicality, chaoticity or entropy of quantum states [16, 18, 21], and have some relevance in various contexts, such as for the characterization of quantum phase transitions [20, 21]. Importantly,

Wehrl moments are experimentally accessible quantities, either from projection measurements of collective observables [17] or heterodyne measurements [19, 22] (see also discussion of possible experimental realizations in Ref. [23]). By contrast, a precise direct experimental determination of the GME is difficult and its calculation, even for pure symmetric states, cannot generally be performed analytically and requires numerical optimisation. A good estimate of the GME on the basis of more readily available partial information than the full quantum state is therefore of theoretical and practical interest, and motivates our approach. In this work, assuming the knowledge of a few Wehrl moments of a set of symmetric multiqubit states, we present and compare three different approaches to estimate their GME, one of which being an ANN that we found to be the most efficient. Note that similar but distinct issues to the one addressed in this work have recently been studied with respect to the detection and certification of entanglement from the Peres-Horodecki criterion based on the first moments of the partial transpose of a state [24, 25]

Our paper is organised as follows. In Sec. 2, we define the Husimi function, the Wehrl moments, the GME and their relations to each other for symmetric multiqubit states. In Sec. 3, we present how we generated the datasets of Wehrl moments used throughout this work. In Sec. 4, we introduce the three different approaches to estimate the GMEs of the dataset: i) a first one based on the two highest known successive Wehrl moments, ii) a second one based on a convergence acceleration algorithm applied on the sequence of the known Wehrl moments and iii) a third one based on a trained ANN. In Sec. 5, we compare and summarize our results. Finally, in Sec. 6, we conclude and present perspectives of our work.

2 Wehrl moments and geometric measure of entanglement

In this section, we define multiqubit symmetric states, the Husimi function and the associated Wehrl moments, the GME, and present how these quantities are related to each other.

2.1 Multiqubit symmetric states

A multiqubit state is said to be symmetric if it is invariant under any permutation of the qubits. Let $|\psi\rangle$ be an N -qubit symmetric state. We can always write this state in terms of N single-qubit normalized states $|\epsilon_i\rangle$ as

$$|\psi\rangle = \mathcal{N}_{|\psi\rangle} \sum_{\sigma \in S_N} |\epsilon_{\sigma(1)}\rangle \otimes |\epsilon_{\sigma(2)}\rangle \otimes \cdots \otimes |\epsilon_{\sigma(N)}\rangle, \quad (1)$$

where $\mathcal{N}_{|\psi\rangle}$ is a normalization constant. Since a one-qubit state, up to a phase factor, can be represented by a point on the Bloch sphere, any symmetric multi-qubit state can be represented geometrically by a constellation of N points, each associated with one of the $|\epsilon_i\rangle$, on the same sphere [26]. In the following, we will refer to these points as the Majorana points of $|\psi\rangle$.

Alternatively, a symmetric state of N qubits can be expanded in the symmetric Dicke states basis as

$$|\psi\rangle = \sum_{k=0}^N d_k |D_N^{(k)}\rangle, \quad (2)$$

where the symmetric Dicke states $|D_N^{(k)}\rangle$ are given by Eq. (1) with $|\epsilon_i\rangle = |1\rangle$ for $i = 1, \dots, k$ and $|\epsilon_i\rangle = |0\rangle$ for $i = k + 1, \dots, N$. The states $|D_N^{(k)}\rangle$ can be thought as angular momentum eigenstates once we introduce the collective spin operators associated with the N -qubit system,

$J_k = \frac{1}{2} \sum_{i=1}^N \sigma_k^{(i)}$ with $k = x, y, z$ and $\sigma_k^{(i)}$ the Pauli operators σ_k for qubit i . It then holds that $J^2 |D_N^{(k)}\rangle = j(j+1) |D_N^{(k)}\rangle$ and $J_z |D_N^{(k)}\rangle = m |D_N^{(k)}\rangle$ with $j = N/2$ and $m = N/2 - k$.

2.2 Husimi function and Wehrl moments

2.2.1 Husimi function

For a spin j , the Husimi function of an arbitrary state $|\psi_j\rangle$ is defined as $Q_{|\psi_j\rangle}(\Omega) = |\langle\psi_j|\Omega\rangle|^2$, where $|\Omega\rangle$ is a spin-coherent state with Ω specifying a point on the unit sphere of \mathbb{R}^3 [27]. The Husimi function $Q_{|\psi_j\rangle}(\Omega)$ is an infinitely differentiable function on the sphere S^2 . In what follows, we will mainly use the notation $Q_{|\psi_j\rangle}(\theta, \varphi)$ where $\theta \in [0, \pi]$ and $\varphi \in [0, 2\pi[$ are the polar and azimuthal angles associated to a point on the unit sphere. The Husimi function is normalized according to [27]

$$\frac{1}{4\pi} \int_{S^2} Q_{|\psi_j\rangle}(\Omega) d\Omega = \frac{1}{2j+1}. \quad (3)$$

For multiqubit symmetric states, the Husimi function $Q_{|\psi\rangle}(\theta, \varphi)$ of an N -qubit state $|\psi\rangle$ is similarly defined as the overlap squared of $|\psi\rangle$ with a symmetric separable pure state $|\epsilon\rangle^{\otimes N}$ where $\Omega = (\theta, \varphi)$ are the coordinates of the point on the Bloch sphere associated with the *single-qubit* state $|\epsilon\rangle \equiv |\theta, \varphi\rangle$. The Husimi function of any state $|\psi\rangle$ is normalized according to (3) with $|\psi_j\rangle \rightarrow |\psi\rangle$ and $2j \rightarrow N$. Using Eq. (1), we can expand it as

$$Q_{|\psi\rangle}(\theta, \varphi) = (N! \mathcal{N}_{|\psi\rangle})^2 |\langle\epsilon_1|\theta, \varphi\rangle|^2 |\langle\epsilon_2|\theta, \varphi\rangle|^2 \cdots |\langle\epsilon_N|\theta, \varphi\rangle|^2. \quad (4)$$

The Husimi function of three different symmetric states of $N = 8$ qubits are shown in Figure 1.

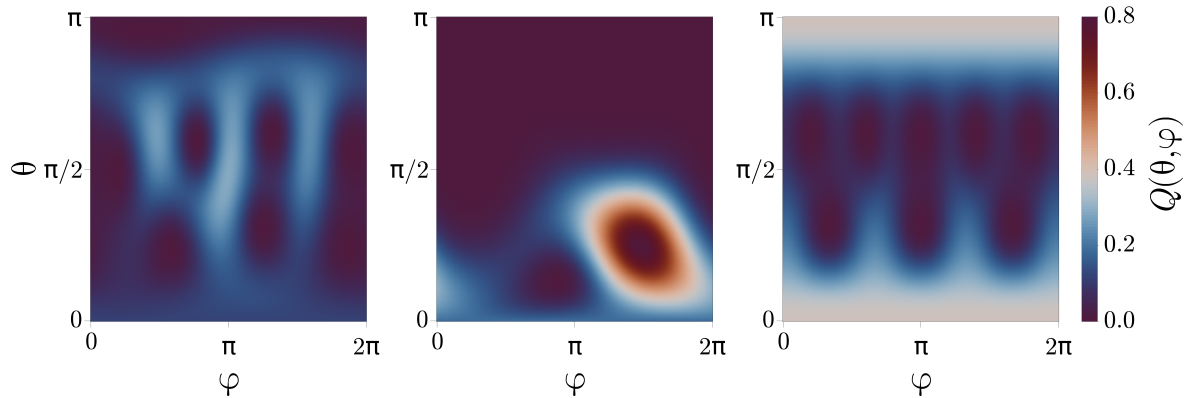


Figure 1: Husimi Q function of symmetric 8-qubit states taken from the three different data subsets introduced in Sec. 3. From left to right (subsets 1 to 3), the GME is 0.717, 0.211 and 0.620 respectively. The more uniform the Husimi function, the higher the GME.

2.2.2 Wehrl moments – explicit expressions

The Wehrl moment $W_{|\psi\rangle}^{(q)}$ of integer order q is the $SU(2)$ invariant defined as

$$W_{|\psi\rangle}^{(q)} = \frac{1}{4\pi} \int_{S^2} (Q_{|\psi\rangle}(\Omega))^q d\Omega. \quad (5)$$

A tight upper bound for Wehrl moments of order $q > 1$ that is valid for any state is given by [27]

$$W_{|\psi\rangle}^{(q)} \leq \frac{1}{Nq + 1}, \quad (6)$$

where the equality holds only for coherent states [28].

An explicit expression for the Wehrl moments of symmetric multiqubit states in terms of expansion coefficients d_k in the Dicke states basis has been given by Gnutzmann and Zyczkowski [16], and reads in our notations

$$W_{|\psi\rangle}^{(q)} = \sum_{m=0}^{qN} \frac{1}{qN + 1} \binom{qN}{m}^{-1} \left| \sum_{i_1, \dots, i_q} \prod_{k=1}^q \sqrt{\binom{N}{i_k}} d_{i_k} \right|^2, \quad (7)$$

where the inner sum goes from 0 to N for each i_k with the restriction $\sum_{k=1}^q i_k = m$. This relation is exact and allows us to calculate the Wehrl moments when we know the expansion (2) of a symmetric state. In Appendix A, we give an alternative expression of Wehrl moments in terms of permanents of Gram matrices of constituent states $\{|\epsilon_i\rangle\}_{i=1}^N$, see Eq. (43). The latter expression is more appropriate when a symmetric state is known in the form of Eq. (1) rather than Eq. (2).

2.3 Geometric measure of entanglement

The geometric measure of entanglement (GME) of an N -qubit pure state $|\psi\rangle$, denoted by $E_G(|\psi\rangle)$, quantifies how far $|\psi\rangle$ is from the set of separable states. Just as the Wehrl moments, it is an $SU(2)$ invariant quantity, defined as [29]

$$E_G(|\psi\rangle) = 1 - \max_{\{|\phi_i\rangle\}_{i=1}^N} |\langle \phi_1 \otimes \phi_2 \cdots \otimes \phi_N | \psi \rangle|^2, \quad (8)$$

where the maximization is performed over the N single-qubit states $|\phi_i\rangle$. The GME is always smaller than 1 and is equal to 0 only when $|\psi\rangle$ is separable. In the case of symmetric states, the maximization appearing in Eq. (8) can be replaced by the simpler maximization where all single qubit states $|\phi_i\rangle$ are identical, i.e. $|\phi_i\rangle = |\epsilon\rangle$ for $i = 1, \dots, N$ [30]. We are thus left with the problem of finding the maximum of the Husimi function of $|\psi\rangle$ on the sphere S^2 , that is

$$\max_{|\epsilon\rangle} |\langle \epsilon \otimes \epsilon \cdots \otimes \epsilon | \psi \rangle|^2 = \max_{\substack{\theta \in [0, \pi] \\ \phi \in [0, 2\pi[}} Q_{|\psi\rangle}(\theta, \varphi). \quad (9)$$

The GME is zero for all product states and non-zero for all entangled states. An (not tight) upper bound on the GME of N -qubit symmetric states is given by [31]

$$E_G(|\psi\rangle) \leq 1 - \frac{1}{N + 1}. \quad (10)$$

2.4 Bounds on GME from Wehrl moments

For any integers $q > p > 1$ and any state $|\psi\rangle$, it holds that

$$\max_{\theta, \phi} Q_{|\psi\rangle} \geq \frac{W_{|\psi\rangle}^{(q+1)}}{W_{|\psi\rangle}^{(q)}} \geq \frac{W_{|\psi\rangle}^{(p+1)}}{W_{|\psi\rangle}^{(p)}}. \quad (11)$$

This is a consequence of the integral Hölder's inequality [32],

$$\|fg\|_1 \leq \|f\|_r \|g\|_m, \quad (12)$$

where $\|f\|_r = \left(\int_X |f|^r d\mu\right)^{\frac{1}{r}}$, $r, m \in [1, \infty]$ with $1/r + 1/m = 1$, and f and g are functions defined on X . By taking $f = Q_{|\psi\rangle}$, $g = Q_{|\psi\rangle}^q$, $X = S^2$, $d\mu = d\Omega/4\pi$, $r = \infty$ and $m = 1$, we readily get Eq. (11) by noting that $\|f\|_\infty = \max_X f$ where $\|\cdot\|_\infty$ denotes the spectral norm. Equation (11) provides us with a chain of better and better upper bounds for the GME as q and p increase. In fact, defining the sequence (for integer $q > 1$)

$$S_{|\psi\rangle}(q) = \frac{W_{|\psi\rangle}^{(q)}}{W_{|\psi\rangle}^{(q-1)}}, \quad (13)$$

we have that

$$E_G(|\psi\rangle) \leq 1 - S_{|\psi\rangle}(q) \quad \forall q > 1, \quad (14)$$

and

$$E_G(|\psi\rangle) = 1 - \max_{\theta, \phi} Q_{|\psi\rangle} = 1 - \|Q_{|\psi\rangle}\|_\infty = 1 - \lim_{q \rightarrow \infty} S_{|\psi\rangle}(q). \quad (15)$$

Equation (15) shows that the geometric measure of entanglement E_G can be extracted from the limit of the sequence $S_{|\psi\rangle}(q)$ of ratios of successive Wehrl moments.

The Wehrl moments admit in some cases simple analytical expressions. For instance, for symmetric Dicke states, they are given by [16]

$$W_{|D_N^{(k)}\rangle}^{(q)} = \frac{\binom{N}{k}^q}{(Nq+1)\binom{Nq}{kq}}. \quad (16)$$

This then leads to

$$1 - E_G(|D_N^{(k)}\rangle) = \lim_{q \rightarrow \infty} S_{|D_N^{(k)}\rangle}(q) = \begin{cases} \binom{N}{k} \left(\frac{k}{N}\right)^k \left(\frac{N-k}{N}\right)^{N-k} & 0 < k < N-1, \\ 1 & k = 0 \vee k = N. \end{cases} \quad (17)$$

in agreement with known results for the geometric entanglement of Dicke states [29]. It is also instructive to analyze how the sequence $S_{|D_N^{(k)}\rangle}(q)$ converges to its limit. From Eq. (16) for $0 < k < N-1$, we find that the sequence $S_{|D_N^{(k)}\rangle}(q)$ is monotonously decreasing and converges asymptotically to its limit as

$$S_{|D_N^{(k)}\rangle}(q) = S_{|D_N^{(k)}\rangle}(\infty) \left[1 - \frac{1}{2q} + \frac{\frac{2}{k-N} - \frac{2}{k} + \frac{26}{N} - 3}{24q^2} + \mathcal{O}\left(\frac{1}{q^3}\right) \right]. \quad (18)$$

For separable states ($k = 0$ or $k = N$), we have [16]

$$W_{\text{coh}}^{(q)} = \frac{2j+1}{2qj+1} \Rightarrow \lim_{q \rightarrow \infty} S_{\text{coh}}(q) = 1, \quad (19)$$

and

$$S_{\text{coh}}(q) = S_{\text{coh}}(\infty) \left[1 - \frac{1}{q} + \frac{1}{Nq^2} + \mathcal{O}\left(\frac{1}{q^3}\right) \right]. \quad (20)$$

In both cases, the dominant correction scales as $1/q$.

The asymptotic scaling as $1/q$ of the dominant correction of $S_{|\psi\rangle}(q)$ is actually a general feature of the sequence valid for *any* state $|\psi\rangle$. Indeed, the asymptotic scaling of the Wehrl moments (5) can be calculated using Laplace's method (see Appendix B for a detailed derivation) and reads

$$W_{|\psi\rangle}^{(q)} = c_{|\psi\rangle} \frac{\|Q_{|\psi\rangle}\|_{\infty}^q}{q} (1 + o(1)), \quad (21)$$

where $c_{|\psi\rangle}$ is a constant independent of q and $o(\cdot)$ the little-o notation [33]. From the definition (13) and properties of the little-o and Big-o, we get

$$S_{|\psi\rangle}(q) = \|Q_{|\psi\rangle}\|_{\infty} \left(1 + \mathcal{O}\left(\frac{1}{q}\right)\right) \quad \forall |\psi\rangle. \quad (22)$$

In Section 4.2, we show how to generalize this analysis and how to take advantage of the knowledge of the asymptotic behavior of the sequence $S_{|\psi\rangle}(q)$ to estimate its limit from a finite number of terms.

3 Datasets and performance metrics

As our objective is to compare different methods to determine the best estimate of the GME of a state from its first few Wehrl moments, we need a set of representative multiqubit states on which to test these methods and calculate some metrics to compare their respective performances (see Sec. 4). This section aims to explain how we generated these representative multiqubit states and what our performance measures are.

3.1 Generation of datasets

In order to obtain a dataset with the most distributed GME values, we generate three different subsets of states. Subset 1 is made of symmetric states with randomly and uniformly distributed Majorana points on the Bloch sphere. Subset 2 is made of random states for which *degenerated* Majorana points are uniformly distributed on the Bloch sphere, with random degeneracy tuples drawn uniformly from all partitions of N . Finally, the subset 3 is made of superpositions of $|\text{GHZ}\rangle = (|D_N^{(0)}\rangle + |D_N^{(N)}\rangle)/\sqrt{2}$ and Dicke states, i.e.

$$|\psi(\alpha, k)\rangle = \mathcal{N} \left[\alpha |\text{GHZ}\rangle + (1 - \alpha) |D_N^{(k)}\rangle \right], \quad (23)$$

with random real number $\alpha \in [0, 1]$ and random integer k between 0 and N . For each number of qubits N , 20000 states are randomly drawn for each subset. All these states are then divided into two equally sized sets: one for training the ANN and the other for testing the three different methods in the estimation of the GME. The Wehrl moments up to $q_{\max} = 8$ and E_G are computed for all states.

Figure 2 shows the GME probability distribution of training states (top) and test states (bottom) for $N = 8$. We find that these three subsets have very different entanglement distributions and are therefore a good set of training and test data. In particular, subset 2 (yellow histograms) is mostly made up of weakly entangled states, while subset 3 (red histograms) contains a significant proportion of very highly entangled states.

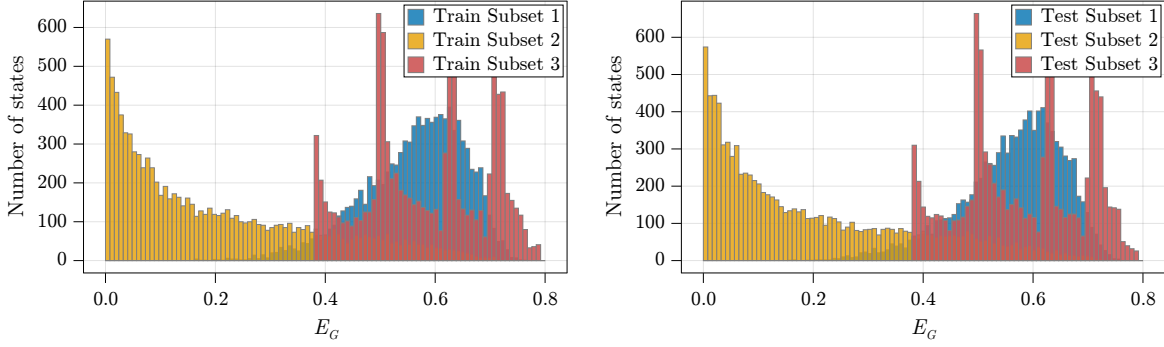


Figure 2: Frequency distributions of GME of the training set (left) and test set (right) for $N = 8$ qubits, where the three subsets of states are represented by different colors. The number of states in the data sets is large enough to generate a similar GME distribution for the training and test sets. For $N = 8$, the maximal GME is $E_G \approx 0.816$ [34], while Eq. (10) gives the upper bound $E_G(|\psi\rangle) \leq 8/9 \approx 0.889$.

3.2 Performance metrics

In order to compare the different methods to estimate the GME, such as convergence acceleration processes and ANNs, we first define the relative difference between the predicted GME and the actual GME as

$$\delta_i = \frac{E_G(|\psi_i\rangle) - E_G^{\text{pred}}(|\psi_i\rangle)}{E_G(|\psi_i\rangle)}, \quad (24)$$

where $E_G^{\text{pred}}(|\psi_i\rangle)$ stands for the predicted GME of state $|\psi_i\rangle$ of the test dataset. Then, we define the mean absolute relative difference, hereafter called *mean relative error* (MRE),

$$\Delta = \frac{1}{M} \sum_{i=1}^M |\delta_i|, \quad (25)$$

where we sum over all states of the test dataset of size $M = 30\,000$. As the distribution of the absolute relative difference $|\delta_i|$ is not Gaussian, the standard deviation is not a good estimate for error bars. Instead, we calculate a low error bar and a high error bar so as to include 68.2% of the $|\delta_i|$ distribution in the error bar and have 15.9% of the distribution below (above) the low (high) error bar, as would be the case for an interval of one standard deviation centred around the mean for a Gaussian distribution.

4 Estimation of the geometric measure of entanglement

In this section, we estimate the GME of the states of the test dataset presented previously based on the knowledge of their Wehrl moments from $q = 1, \dots, q_{\text{max}}$, expecting a better estimate of the GME as q_{max} increases. We use and compare three different methods: i) a crude one based on the ratio of the two highest known Wehrl moments, ii) a second one based on a convergence acceleration algorithm applied on the set of known Wehrl moments and iii), a third one based on a trained ANN. We are particularly interested in the performance of the different methods as a function of the highest considered order q_{max} and of the number of qubits N .

4.1 Wehrl moments ratios

As the ratios of successive Wehrl moments (13) converge to the maximum of the Husimi function when $q \rightarrow \infty$ [see Eq. (15)], a first estimate of the GME of the test states based on these ratios is given by

$$E_G^{\text{pred}}(|\psi\rangle) = 1 - S_{|\psi\rangle}(q_{\text{max}}). \quad (26)$$

The predictive power of (26) is illustrated in Fig. 3 for different maximal orders q_{max} and number of qubits N . As expected from the inequality (14), we observe that the estimate (26) is always larger than the actual value of the GME (left panels), which results in a positive relative difference (middle panels). As q_{max} increases, the estimate becomes better and better, with a decrease in mean relative error (MRE) as a function of q_{max} (top right panel). However, even with $q_{\text{max}} = 8$, the MRE remains above 10%. The MRE increases slightly with N before stabilising quickly, as shown in the bottom right panel.

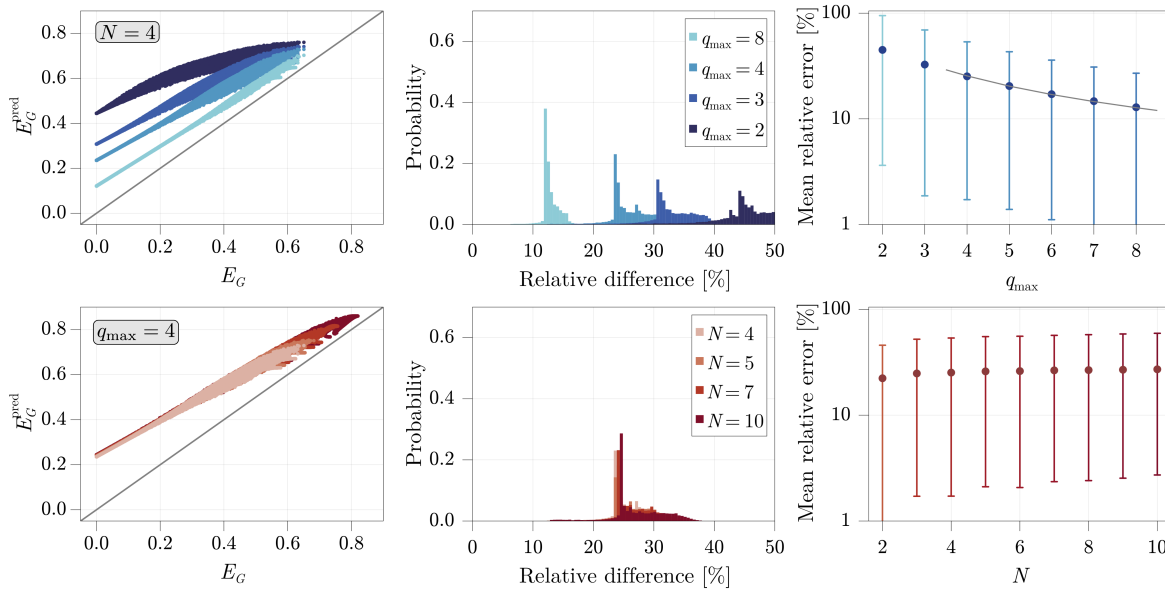


Figure 3: Predictions of E_G based directly on Wehrl moment ratios $S_{|\psi\rangle}(q_{\text{max}}) = W_{|\psi\rangle}^{(q_{\text{max}})}/W_{|\psi\rangle}^{(q_{\text{max}}-1)}$ for $N = 4$ and different maximal orders q_{max} (top) and for $q_{\text{max}} = 4$ and different number of qubits N (bottom). Left panels: Predicted value versus actual value of GME for all states of the test dataset. Middle panels: Probability to predict the GME with a certain relative difference. The bins size is 0.5%. Right panels: Mean relative error (25) as a function of q_{max} and N . The grey solid line in the top right panel shows a fit of equation $\Delta(q_{\text{max}}) = A/q_{\text{max}}$ with $A \approx 102$, which is the expected behaviour at large q_{max} according to Eq. (22).

4.2 Convergence acceleration algorithms

Convergence acceleration algorithms consist in transforming a sequence into another sequence that converges faster to its limit, by taking as inputs only the first terms of the original sequence. Different algorithms exist in the literature and differ from each other depending on how the terms of the initial sequence are combined together to generate the new sequence. We focus here on

the use of the recursive E -algorithm [35], which is among the algorithms we tested the one that showed the best performance. Our goal, by applying it on the sequence $S_{|\psi\rangle}(q)$ [Eq. (13)], is to obtain a better estimate of its limit $S_{|\psi\rangle}(\infty)$, and thus of the GME of the states through Eq. (15).

The recursive E -algorithm makes it possible to accelerate sequences $f(q)$ with asymptotic expansions of the general form

$$f(q) = f(\infty) \left[1 + \lambda_1 g_1(q) + \lambda_2 g_2(q) + \lambda_3 g_3(q) + \dots \right], \quad (27)$$

where $g_i(q)$ are known (or postulated) scaling functions ordered such that

$$\lim_{q \rightarrow \infty} \frac{g_{i+1}(q)}{g_i(q)} = 0 \quad \forall i, \quad (28)$$

i.e., so that $g_1(q)$ corresponds to the dominant asymptotic scaling of the sequence $f(q)$, and with arbitrary (and potentially unknown) coefficients λ_i . According to the recursive E -algorithm, a better estimate of the limit $f(\infty)$ can be obtained by computing via recurrence the quantities

$$E_k^{(q)} = \frac{E_{k-1}^{(q)} g_{k-1,k}^{(q+1)} - E_{k-1}^{(q+1)} g_{k-1,k}^{(q)}}{g_{k-1,k}^{(q+1)} - g_{k-1,k}^{(q)}}, \quad (29)$$

taking $E_0^{(q)} = f(q)$ as the initial conditions and the coefficients

$$g_{k,i}^{(q)} = \frac{g_{k-1,i}^{(q)} g_{k-1,k}^{(q+1)} - g_{k-1,i}^{(q+1)} g_{k-1,k}^{(q)}}{g_{k-1,k}^{(q+1)} - g_{k-1,k}^{(q)}}, \quad g_{0,i}^{(q)} = g_i(q), \quad \forall k \in \mathbb{N}_0, i \geq k+1. \quad (30)$$

A quick inspection shows that $E_k^{(q)}$ is a function of the set $\{f(q), f(q+1), \dots, f(q+k)\}$. In practice, increasing the order k of the algorithm generally provides a better estimate $E_k^{(q)}$ of the limit $f(\infty)$ of the initial sequence $f(q)$, but requires knowing and combining more terms of the sequence.

The recursive E -algorithm is particularly suited for the acceleration of the sequence $S_{|\psi\rangle}(q)$ for which we have an idea of the form of the scaling functions $g_i(q)$ defined in Eq. (27). Indeed, motivated by the general asymptotic behaviour of $S_{|\psi\rangle}(q)$ given by Eq. (22) and the two particular cases (18) and (20) studied in Sec. 2.4, we consider here the following ansatz:

$$S_{|\psi\rangle}(q) = S_{|\psi\rangle}(\infty) \left(1 + \frac{\lambda_1}{q} + \frac{\lambda_2}{q^2} + \frac{\lambda_3}{q^3} + \dots \right), \quad (31)$$

i.e., the general expansion (27) with $g_i(q) = q^{-i}$.

In Fig. 3, we showed the GMEs of the states of the test dataset via the crude estimate $S_{|\psi\rangle}(q_{\max})$. In order to have a fair comparison, we estimate here the GMEs of these states with $E_{q_{\max}-2}^{(2)}$, which exploits all the first terms of the sequence $S_{|\psi\rangle}(q)$ up to $q = q_{\max}$, i.e., $\{S_{|\psi\rangle}(q) : q = 2, \dots, q_{\max}\}$. Figure 4 shows the results for different N and q_{\max} . As expected, the estimates of the GME is better than the crude estimate $S_{|\psi\rangle}(q_{\max})$ with the convergence acceleration algorithm, especially for low q_{\max} . In particular, the skewness of the distributions of predicted GMEs compared to actual GMEs is much less pronounced. For $N = 4$, we can see in the top right panel that the MRE is already reduced to only about 10% for $q_{\max} = 3$ [one order of magnitude lower than for the estimate $1 - S_{|\psi\rangle}(q_{\max})$]. For larger q_{\max} , we find a behaviour compatible with an exponential decrease of the RME.

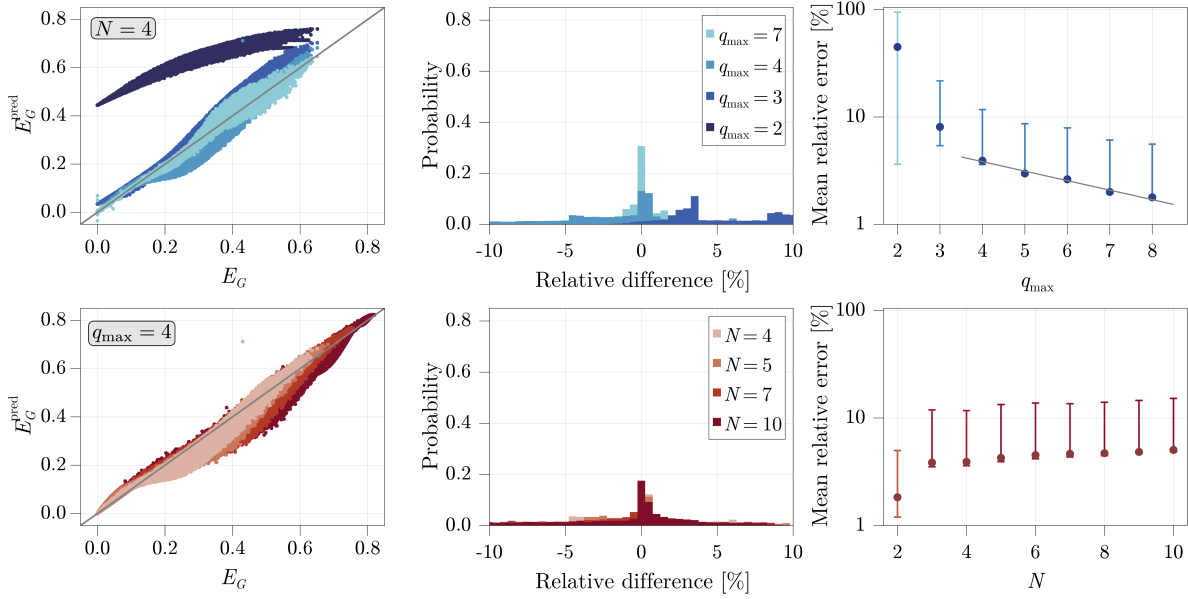


Figure 4: Same representation and parameters as in Fig. 3, but with predictions based on the recursive E -algorithm. The grey solid line in the top right panel shows a decreasing exponential fit of equation $\Delta(q_{\max}) \approx 8.667 \exp(-0.204 q_{\max})$.

Note that we also compared the results of the E -algorithm to the ones obtained via the implementation of the θ -algorithm, a popular convergence acceleration algorithm which has the advantage to not require the knowledge of the asymptotic scaling of the accelerated sequence, but we did not find better performance (data not shown).

4.3 Artificial Neural Networks

We now want to train artificial neural networks (ANNs) so that when we feed them with the finite sequence

$$\{S_{|\psi\rangle}(q) : q = 2, \dots, q_{\max}\}$$

for some state $|\psi\rangle$, they output an estimate for $E_G(|\psi\rangle) = 1 - \lim_{q \rightarrow \infty} S_{|\psi\rangle}(q)$, as schematically represented in Fig. 5. To be able to compare the trainings based on different q_{\max} and N , we choose to always use the same network architecture

$$(q_{\max} - 1, 512, \text{ReLU}, 256, \text{ReLU}, 128, \text{ReLU}, 64, \text{ReLU}, 32, \text{ReLU}, 1) \quad (32)$$

where ReLU is the Rectified Linear Unit as used in deep learning [36]. For the learning process, we take a batch size of 500 and, for each $q_{\max} \in [2, 8]$ and $N \in [2, 10]$, we train the ANN in a supervised manner for 5000 epochs with ADAM optimizer. Our loss function is the squared difference averaged over the batch. Remarkably, even after 5000 epochs, no overfitting is observed (see Fig. 8 and the additional discussion in Appendix C).

We show in Fig. 6 the results of the different trainings applied to the test dataset. We find that ANNs give quite reliable predictions already for $q_{\max} = 3$ with a MRE at 1%, one order of magnitude less than with the convergence acceleration. More surprisingly, even on the basis of the first non-trivial Wehrl moment $W_{|\psi\rangle}^{(2)}$, ANNs give a good estimate for weakly and strongly entangled states. As we take more input, i.e. Wehrl moments, ANNs are able to predict the GME

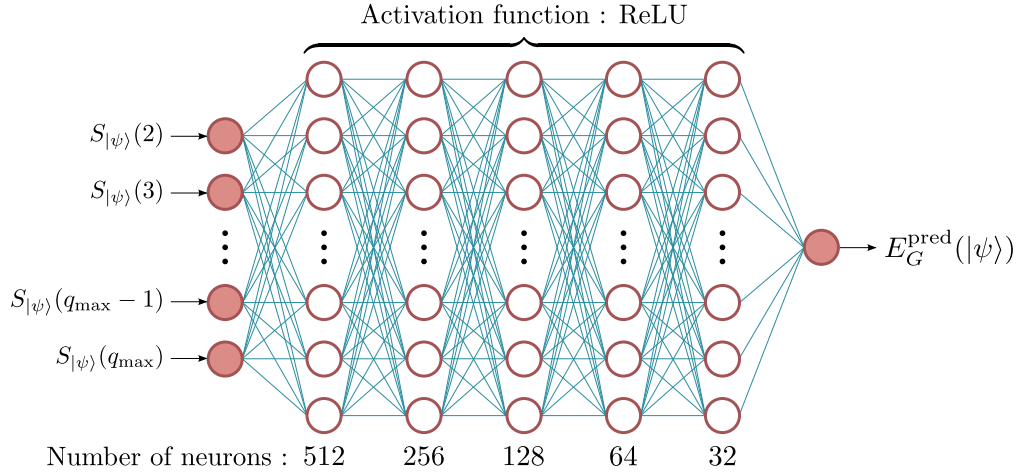
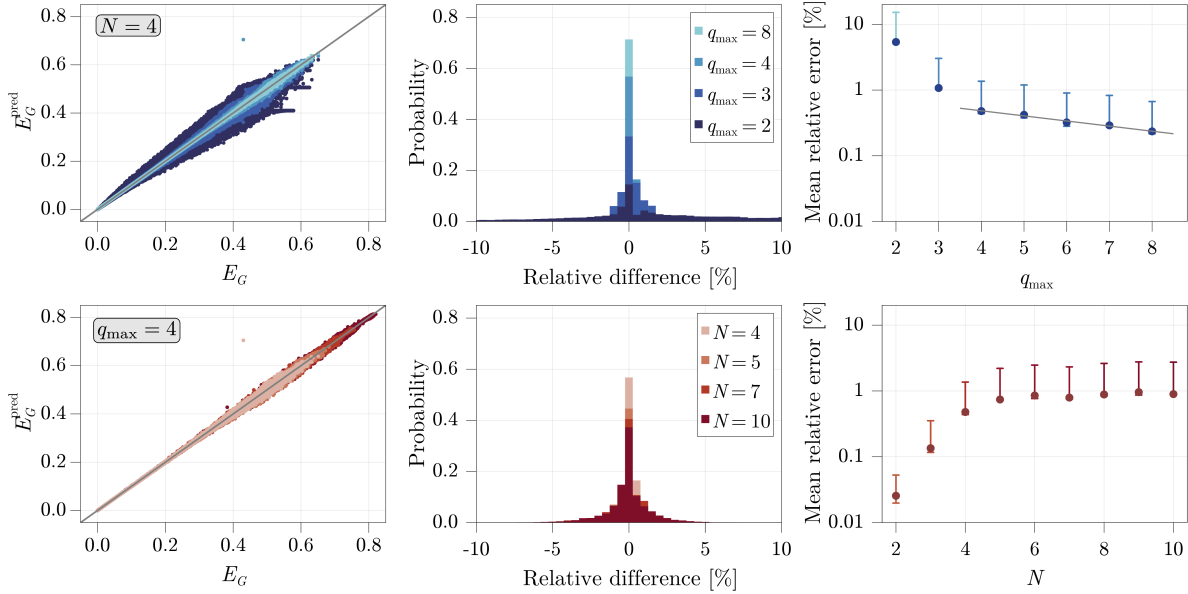


Figure 5: Representation of the ANN architecture used in this work.


 Figure 6: Same representation and parameters as in Fig. 3, but with predictions based on trained ANNs. The grey solid line in the top right panel shows a decreasing exponential fit of equation $\Delta(q_{\max}) \approx 0.989 \exp(-0.179 q_{\max})$.

more accurately. We also observe that at fixed $q_{\max} = 4$, the RME first increases with the number of qubits and then saturates at roughly 1%. This is probably due to the fact that entanglement can take more complex forms for a higher number of qubits.

5 Discussion

We will now summarise our main results. We show in Fig. 7 the mean relative error for the different methods investigated in Sec. 4, for a wide range of maximum orders q_{\max} and number of qubits N . The relative performance of the different methods of obtaining estimates for the GME

are clearly evident. We consistently find that the MRE on the GME is lowest for the ANNs, then for the convergence acceleration algorithm and finally for the Wehrl moment ratios. The differences in performance are quite large, with ANNs outperforming the other methods by at least an order of magnitude. For the methods based on ANNs and convergence acceleration algorithms, the MRE decreases very rapidly from $q_{\max} = 2$ to $q_{\max} = 4$. Then, the MRE decreases exponentially at roughly the same rate for both methods. For $q_{\max} = 4$, the MRE obtained with ANNs seems to quickly saturate to about 1% for large number of qubits ($N \gtrsim 6$, see right panel). We have also tested the ANN on a set of states that have been dynamically generated from spin squeezing. This set is characterised by a GME distribution that differs strongly from those used to train the ANN (see appendix C for more details). In this case, we find that the ANN also works very well with similar performance, demonstrating its great flexibility upon variations of input data.

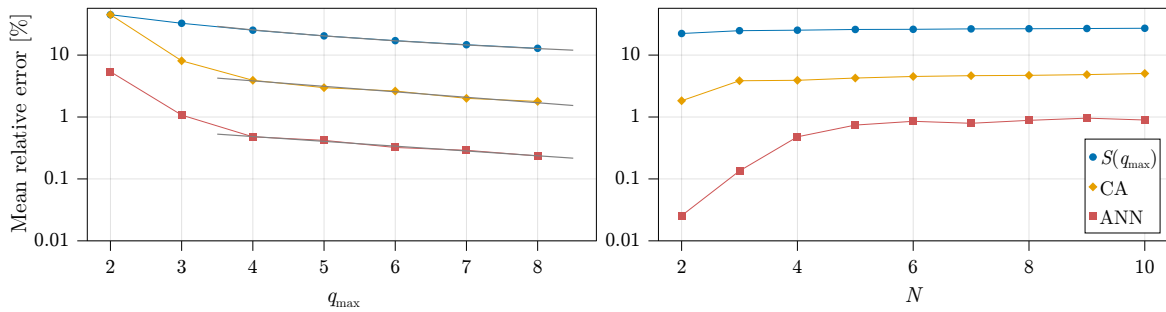


Figure 7: Comparison of the mean relative error (MRE) on the GME obtained with the bare Wehrl moment ratios (blue dots), with the recursive E -algorithm for convergence acceleration (yellow diamonds) and with ANNs (red squares). Left panel: MRE as a function of q_{\max} for $N = 4$. Right panel: MRE as a function of N for $q_{\max} = 4$.

6 Conclusion

In this work, we have studied how ANNs can be used to give an accurate estimate of the geometric measure of entanglement (GME) of symmetric multiqubit states based on their first Wehrl moments (moments of their Husimi function). We also used convergence acceleration methods to estimate the GME. More specifically, we implemented the algorithm E informed by the asymptotic behaviour of the Wehrl moments which we determined analytically. We found that even this powerful convergence acceleration algorithm is outperformed by ANNs when fed with the same input data. This gives prospects for the estimation and certification of entanglement based on a few Wehrl moments.

This work opens up several perspectives. First, while we have focused on the determination of GME, our approach could have been used to determine e.g. the Wehrl entropy [44, 45], as both GME and such entropy are based on Wehrl moments, opening up characterizations of quantum chaos and phase transitions via ANNs. In addition, it is known that the determination of the GME of mixed states is considerably more complex than that of pure states. But as a mixed symmetric state ρ is completely characterized by its Husimi function, $Q_\rho(\Omega) = \langle \Omega | \rho | \Omega \rangle$, it would be worth investigating the extent to which it is possible to estimate its entanglement (or other $SU(2)$ -invariant) as we have done in this work, which would be particularly relevant as most experimental platforms deal with open quantum systems due to the unavoidable coupling to the

environment. The generalization of our approach to non-symmetric many-body states, for which one faces the exponential many-body wall, is also an important and promising perspective, as one can expect some advantages when using ANNs in this context [46]. More generally, an approach similar to the one used in this work could be followed to estimate the maximum or minimum of a continuous (quasi)probability distribution other than the Husimi function from its first moments, such as the Wigner function in order to explore non-classicality of quantum states.

Acknowledgements

Most of the computations were done with the Julia programming language, in particular using the Flux.jl package [37]. The figures were produced with the package Makie [38].

Author contributions JM conceived the presented idea, made the general theoretical developments and supervised the project. JD and FD carried out the developments and computations relating to the ANN and the acceleration of convergence, respectively. All authors discussed the results and their analysis at all stages of the work and contributed to the writing of the manuscript.

Funding information Computational resources were provided by the Consortium des Equipements de Calcul Intensif (CECI), funded by the Fonds de la Recherche Scientifique de Belgique (F.R.S.-FNRS) under Grant No. 2.5020.11. FD acknowledges the Belgian F.R.S.-FNRS for financial support during this work.

A Explicit expression of Wehrl moments in terms of $|\epsilon_i\rangle$

Suppose we are given a symmetric state in the form of Eq. (1), i.e. in terms of normalized single-qubit states $|\epsilon_i\rangle$ (hereinafter referred to as constituent states) as

$$|\psi\rangle = \mathcal{N}_{|\psi\rangle} \sum_{\sigma \in S_N} |\epsilon_{\sigma(1)}\rangle \otimes |\epsilon_{\sigma(2)}\rangle \otimes \cdots \otimes |\epsilon_{\sigma(N)}\rangle, \quad (33)$$

where the normalization constant $\mathcal{N}_{|\psi\rangle}$ is given by

$$\mathcal{N}_{|\psi\rangle}^{-2} = N! \sum_{\sigma \in S_N} \langle \epsilon_1 | \epsilon_{\sigma(1)} \rangle \cdots \langle \epsilon_N | \epsilon_{\sigma(N)} \rangle. \quad (34)$$

In this Appendix, we show how to obtain an expression for the Wehrl moments directly in terms of the $|\epsilon_i\rangle$. First, let $G_{|\psi\rangle}$ be the matrix of overlaps between the single-qubit states, that is,

$$G_{|\psi\rangle} = \begin{pmatrix} \langle \epsilon_1 | \epsilon_1 \rangle & \cdots & \langle \epsilon_1 | \epsilon_N \rangle \\ \vdots & \ddots & \vdots \\ \langle \epsilon_N | \epsilon_1 \rangle & \cdots & \langle \epsilon_N | \epsilon_N \rangle \end{pmatrix}. \quad (35)$$

The matrix (35) is nothing but the Gram matrix of the constituent states $\{|\epsilon_i\rangle\}_{i=1}^N$, which was also introduced in Ref. [39] in connection with the problem of determining the geometric measure of entanglement of symmetric states. Then the normalization constant can be expressed as [40, 41]

$$\mathcal{N}_{|\psi\rangle}^{-2} = N! \text{per}(G_{|\psi\rangle}) \iff \mathcal{N}_{|\psi\rangle} = \frac{1}{\sqrt{N! \text{per}(G_{|\psi\rangle})}}, \quad (36)$$

where $\text{per}(A)$ denotes the permanent of the matrix A , defined as

$$\text{per}(A) = \sum_{\sigma \in S_N} \prod_{i=1}^N A_{i\sigma(i)}. \quad (37)$$

After these preliminary developments, let us show how to obtain the desired explicit expression for the Wehrl moments. Some of our reasoning follows similar lines to those in Ref. [42]. We begin by noting that any integer power q of the Husimi function (4) can be written as

$$Q_{|\psi\rangle}^q(\theta, \varphi) = (N! \mathcal{N}_{|\psi\rangle})^{2q} \underbrace{|\langle \epsilon_1 | \theta, \varphi \rangle|^2 \cdots |\langle \epsilon_1 | \theta, \varphi \rangle|^2}_{q \text{ times}} \cdots \underbrace{|\langle \epsilon_N | \theta, \varphi \rangle|^2 \cdots |\langle \epsilon_N | \theta, \varphi \rangle|^2}_{q \text{ times}}. \quad (38)$$

with $|\theta, \varphi\rangle$ the state of a qubit whose corresponding point on the Bloch sphere has coordinates (θ, φ) . Based on Eq. (4), it is easy to see that, up to a multiplicative constant, Eq. (38) is the Husimi function of the (Nq) -qubit symmetric state $|\psi_q\rangle$ with the same constituent states $|\epsilon_i\rangle$ as $|\psi\rangle$ but each now appearing q times (i.e. each state $|\epsilon_i\rangle$ is q -fold degenerated). Indeed, it holds that

$$Q_{|\psi_q\rangle}(\theta, \varphi) = ((Nq)! \mathcal{N}_{|\psi_q\rangle})^2 |\langle \epsilon_1 | \theta, \varphi \rangle|^{2q} \cdots |\langle \epsilon_N | \theta, \varphi \rangle|^{2q} \quad (39)$$

from which follows the relation

$$Q_{|\psi\rangle}^q(\theta, \varphi) = \frac{(N! \mathcal{N}_{|\psi\rangle})^{2q}}{((Nq)! \mathcal{N}_{|\psi_q\rangle})^2} Q_{|\psi_q\rangle}(\theta, \varphi). \quad (40)$$

Then, since the Husimi function $Q_{|\psi_q\rangle}(\theta, \varphi)$ obeys the normalization condition

$$\frac{1}{4\pi} \int Q_{|\psi_q\rangle}(\Omega) d\Omega = \frac{1}{Nq+1}, \quad (41)$$

we have

$$W_{|\psi\rangle}^{(q)} = \frac{1}{4\pi} \int Q_{|\psi\rangle}^q(\Omega) d\Omega = \frac{(N! \mathcal{N}_{|\psi\rangle})^{2q}}{((Nq)! \mathcal{N}_{|\psi_q\rangle})^2} \frac{1}{Nq+1} \quad (42)$$

or, finally, by using Eq. (36)

$$W_{|\psi\rangle}^{(q)} = \frac{\text{per}(G_{|\psi_q\rangle})}{(\text{per}(G_{|\psi\rangle}))^q} \frac{(N!)^q}{(Nq+1)!} \quad (43)$$

where $G_{|\psi\rangle}$ is the Gram matrix (35) and $G_{|\psi_q\rangle}$ is a Gram matrix made of $q \times q$ identical blocks $G_{|\psi\rangle}$ as follows

$$G_{|\psi_q\rangle} = \begin{pmatrix} G_{|\psi\rangle} & \cdots & G_{|\psi\rangle} \\ \vdots & \ddots & \vdots \\ G_{|\psi\rangle} & \cdots & G_{|\psi\rangle} \end{pmatrix}. \quad (44)$$

Equation (43) is our exact result for the Wehrl moments as a function of the constituent states $|\epsilon_i\rangle$ that appear in Eq. (1).

B Asymptotic behaviour of the Wehrl moments

In this Appendix, we derive the asymptotic scaling of the Wehrl moments, Eq. (49), using Laplace's approximation for evaluating integrals, following [43].

First, let us rewrite without restriction the Wehrl moments (5) as

$$W_{|\psi\rangle}^{(q)} = \frac{1}{4\pi} \int_{S^2} e^{-q f_{|\psi\rangle}(\Omega)} d\Omega. \quad (45)$$

where $f_{|\psi\rangle}(\Omega) = -\ln(Q_{|\psi\rangle}(\Omega))$ is a function $f : S^2 \rightarrow \mathbb{R}$. For large q , we expect the integrand to be non-negligible only around the minimum of $f_{|\psi\rangle}(\Omega)$ (the maximum of $Q_{|\psi\rangle}(\Omega)$). For simplicity, we consider here the generic case where the minimum is unique, which is however not the case for all states. The idea to obtain the asymptotic behavior of the Wehrl moments as $q \rightarrow \infty$ is to perform a series expansion of $f_{|\psi\rangle}(\Omega)$ around its minimum. For convenience, we expand instead the function $\tilde{f}_{|\psi\rangle}(\Omega) = [f_{|\psi\rangle}(\Omega) - f_{|\psi\rangle}(\Omega^*)] / f_{|\psi\rangle}''(\Omega^*)$ around Ω^* , the value of $\Omega = (\theta, \varphi)$ minimizing $f_{|\psi\rangle}(\Omega)$, where $f_{|\psi\rangle}''(\Omega)$ the Hessian matrix of $f(\Omega)$. Since $\tilde{f}_{|\psi\rangle}(\Omega^*) = 0$ and $\tilde{f}_{|\psi\rangle}''(\Omega) = \mathbb{1}$ where $\mathbb{1}$ is the identity matrix, the expansion of $\tilde{f}_{|\psi\rangle}(\Omega)$ around Ω^* simply reads

$$\tilde{f}_{|\psi\rangle}(\Omega) = \frac{1}{2} \|\Omega - \Omega^*\|^2 + o(\|\Omega - \Omega^*\|^2) = \frac{1}{2} \|\Omega - \Omega^*\|^2 (1 + o(1)) \quad (46)$$

where $\|\cdot\|$ is the standard Euclidian norm and $o(\cdot)$ the little-o notation [33]. The Wehrl moment (45) then reads

$$W_{|\psi\rangle}^{(q)} = \frac{1}{4\pi} e^{-q f_{|\psi\rangle}(\Omega^*)} \int_{S^2} e^{-q f_{|\psi\rangle}''(\Omega^*) \frac{\|\Omega - \Omega^*\|^2}{2} (1 + o(1))} d\Omega. \quad (47)$$

By making a change of variable $\tilde{\Omega} = \sqrt{q f_{|\psi\rangle}''(\Omega^*)} (\Omega - \Omega^*)$ where $\sqrt{q f_{|\psi\rangle}''(\Omega^*)}$ is the positive square root of the Hessian matrix $f_{|\psi\rangle}''(\Omega)$, the integral becomes

$$W_{|\psi\rangle}^{(q)} = \frac{e^{-q f_{|\psi\rangle}(\Omega^*)}}{4\pi q \sqrt{\det(f_{|\psi\rangle}''(\Omega^*))}} \int e^{-\frac{\|\tilde{\Omega}\|^2}{2} (1 + o(1))} d\tilde{\Omega} \quad (48)$$

where $\det(\cdot)$ is the determinant. For large q , the region of integration tends to \mathbb{R}^2 , and the integral becomes a standard 2D Gaussian integral equal to $2\pi/(1 + o(1)) = 2\pi(1 + o(1))$. Hence, the asymptotic behavior of the Wehrl moments finally reads

$$W_{|\psi\rangle}^{(q)} = c_{|\psi\rangle} \frac{e^{-q f_{|\psi\rangle}(\Omega^*)}}{q} (1 + o(1)) = c_{|\psi\rangle} \frac{\|Q_{|\psi\rangle}\|_\infty^q}{q} (1 + o(1)) \quad (49)$$

where

$$c_{|\psi\rangle} = \frac{1}{2\sqrt{\det(f_{|\psi\rangle}''(\Omega^*))}} \quad (50)$$

is a constant independent of q .

C Additional information on ANNs

Figure 8 shows an example of the evolution of the loss function on the test dataset throughout the training of the ANN for different numbers of qubits and $q_{\max} = 4$. We observe no overfitting, with the loss function decreasing even after a large number of epochs.

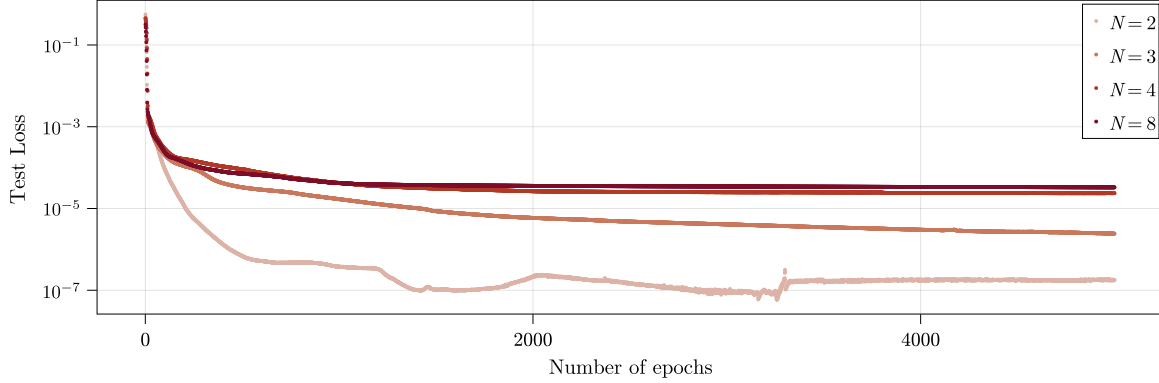


Figure 8: Loss function (averaged squared error, see Sec. 4.3) of the test dataset as a function of the number of training epochs for a maximal order $q_{\max} = 4$ and different numbers of qubits N .

Figure 9 shows the performance of the ANNs for a larger number of qubits and a larger maximal order than the results presented in the main text. For the top panels $N = 8$ and for the bottom panels $q_{\max} = 8$. The same general observations as in the main text apply in this case, in particular the fact that the mean relative error is below 1% already for $q_{\max} = 4$.

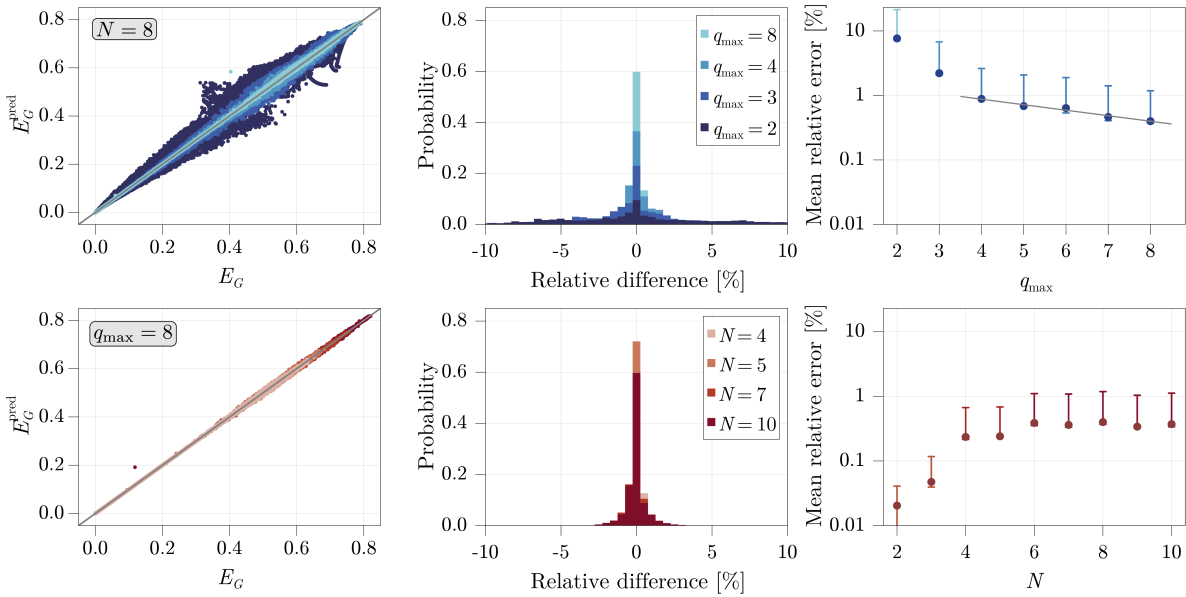


Figure 9: Same as Fig. 6 for $N = 8$ (top) and $q_{\max} = 8$ (bottom). The grey solid line in the top right panel shows a decreasing exponential fit of equation $\Delta(q_{\max}) \approx 1.919 \exp(-0.197 q_{\max})$.

In order to further test the performance of ANNs, we generated another set of states resulting from the dynamical evolution corresponding to a spin squeezing. We calculated the time evolution of the initial coherent/product state $|D_N^{(0)}\rangle$ under the Hamiltonian

$$H = \chi_x J_x^2 + \chi_y J_y^2 + \chi_z J_z^2. \quad (51)$$

where χ_x, χ_y, χ_z are squeezing rates along the three spatial directions. At regular times, we sampled the state of the system and calculated its Wehrl moments and GME. After 500 time steps $\Delta t = 0.1$, we ended the evolution and started again from the same initial state. The χ_α rates were chosen randomly between 0 and 1 at the beginning of each evolution. In this way, we generated 30 000 states on which we tested the previously trained ANNs. The results are presented in Fig. 10. We find that the ANNs still predict E_G very well even though they have never handled this type of states before. This shows that the training set was sufficiently large and representative to obtain ANNs capable of inferring beyond the states on which they have been trained.

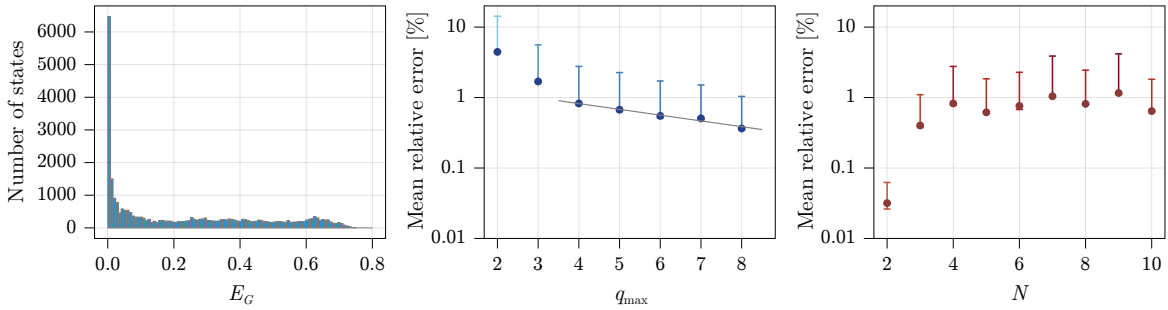


Figure 10: Left panel: Frequency distribution of GME of 30 000 squeezed states generated for $N = 8$ qubits. Middle and right panels: mean relative error on the estimate of the GME obtained from ANNs for $N = 4$ and $q_{\max} = 4$ respectively. The grey solid line shows a decreasing exponential fit of equation $\Delta(q_{\max}) \approx 1.745 \exp(-0.189 q_{\max})$.

References

- [1] A. Acín, I. Bloch, H. Buhrman, T. Calarco, C. Eichler, J. Eisert, D. Esteve, N. Gisin, S. J. Glaser, F. Jelezko, S. Kuhr, M. Lewenstein, M. F. Riedel, P. O. Schmidt, R. Thew, A. Wallraff, I. Walmsley, and F. K. Wilhelm, *The Quantum Technologies Roadmap: A European Community View*, New J. Phys. **20**, 080201 (2018). doi:<https://doi.org/10.1088/1367-2630/aad1ea>
- [2] V. Dunjko and H. J. Briegel, *Machine learning & artificial intelligence in the quantum domain : a review of recent progress*, Rep. Prog. Phys. **81**, 074001 (2018), doi:<https://doi.org/10.1088/1361-6633/aab406>
- [3] G. Carleo, I. Cirac, K. Cranmer, L. Daudet, M. Schuld, N. Tishby, L. Vogt-Maranto, and L. Zdeborová, *Machine learning and the physical sciences*, Rev. Mod. Phys. **91**, 045002 (2019), doi:<https://doi.org/10.1103/RevModPhys.91.045002>
- [4] S. Ahmed, C. S. Muñoz, F. Nori, and A. F. Kockum, *Quantum State Tomography with Conditional Generative Adversarial Networks*, Phys. Rev. Lett. **127**, 140502 (2021), doi:<https://doi.org/10.1103/PhysRevLett.127.140502>

- [5] G. Torlai, G. Mazzola, J. Carrasquilla, M. Troyer, R. Melko, and G. Carleo *Neural-network quantum state tomography*, Nature Phys. **14**, 447 (2018), doi:<https://doi.org/10.1038/s41567-018-0048-5>
- [6] Y. Quek, S. Fort, and H. K. Ng, *Adaptive quantum state tomography with neural networks*, npj Quantum Inf. **7**, 105 (2021), doi:<https://doi.org/10.1038/s41534-021-00436-9>
- [7] V. Cimini, M. Barbieri, N. Treps, M. Walschaers, and V. Parigi, *Neural Networks for Detecting Multimode Wigner Negativity*, Phys. Rev. Lett. **125**, 160504 (2020), doi:<https://doi.org/10.1103/PhysRevLett.125.160504>
- [8] X.-M. Zhang, Z. Wei, R. Asad, X.-C. Yang, and X. Wang, *When does reinforcement learning stand out in quantum control? A comparative study on state preparation*, npj Quantum Inf. **5**, 85 (2019), doi:<https://doi.org/10.1038/s41534-019-0201-8>
- [9] S. Mavadia, V. Frey, J. Sastrawan, S. Dona, and M. J. Biercuk, *Prediction and real-time compensation of qubit decoherence via machine learning*, Nat. Commun. **8**, 14106 (2017), doi:<https://doi.org/10.1038/ncomms14106>
- [10] T. Fösel, P. Tighineanu, T. Weiss, and F. Marquardt, *Reinforcement Learning with Neural Networks for Quantum Feedback*, Phys. Rev. X **8**, 031084 (2018), doi:<https://doi.org/10.1103/PhysRevX.8.031084>
- [11] M. Che, L. Qi, Y. Wei and G. Zhang, *Geometric measures of entanglement in multipartite pure states via complex-valued neural networks*, Neurocomputing **313**, 25 (2018), doi:[10.1016/j.neucom.2018.05.094](https://doi.org/10.1016/j.neucom.2018.05.094)
- [12] D. Koutný, L. Ginés, M. Moczala-Dusanowska, S. Höfling, C. Schneider, A. Predojević, and Miroslav Ježek, *Deep learning of quantum entanglement from incomplete measurements*, arXiv:2205.01462 (2022), doi:<https://doi.org/10.48550/arXiv.2205.01462>
- [13] C. Harney and S. Pirandola and A. Ferraro and M. Paternostro, *Entanglement classification via neural network quantum states*, New Journal of Physics **22**, 045001 (2020), doi:[10.1088/1367-2630/ab783d](https://doi.org/10.1088/1367-2630/ab783d)
- [14] C. Harney and M. Paternostro and S. Pirandola *Mixed state entanglement classification using artificial neural networks*, New Journal of Physics **23**, 063033 (2021), doi:<https://doi.org/10.1088/1367-2630/ac0388>
- [15] R. Berkovits, *Extracting many-particle entanglement entropy from observables using supervised machine learning*, Phys. Rev. B. **98**, 241411 (2018), doi:[10.1103/PhysRevB.98.241411](https://doi.org/10.1103/PhysRevB.98.241411)
- [16] S. Gnutzmann and K. Zyczkowski, *Rényi-Wehrl entropies as measures of localization in phase space*, J. Phys. A: Math. Gen. **34**, 10123 (2001), doi:[10.1088/0305-4470/34/47/317](https://doi.org/10.1088/0305-4470/34/47/317)
- [17] M. A. Perlin, D. Barberena, and A. M. Rey, *Spin qudit tomography and state reconstruction error*, Phys. Rev. A **104**, 062413 (2021), doi:<https://doi.org/10.1103/PhysRevA.104.062413>
- [18] A. Sugita and H. Aiba, *Second moment of the Husimi distribution as a measure of complexity of quantum states*, Phys. Rev. E **65**, 036205 (2002), doi:<https://doi.org/10.1103/PhysRevE.65.036205>

- [19] V. Buzek, C. H. Keitel, and P. L. Knight, *Sampling entropies and operational phase-space measurement. I. General formalism*, Phys. Rev. A **51**, 2575 (1995), doi:<https://doi.org/10.1103/PhysRevA.51.2575>
- [20] B. O. Goes, G. T. Landi, E. Solano, M. Sanz, and L. C. Céleri, *Wehrl entropy production rate across a dynamical quantum phase transition*, Phys. Rev. Research **2**, 033419 (2020), doi:<https://doi.org/10.1103/PhysRevResearch.2.033419>
- [21] E. Romera, R. del Real, M. Calixto, *Husimi distribution and phase-space analysis of a Dicke-model quantum phase transition*, Phys. Rev. A **85**, 053831 (2012), doi:<https://doi.org/10.1103/PhysRevA.85.053831>
- [22] E. V. Shchukin and W. Vogel, *Nonclassical moments and their measurement*, Phys. Rev. A **72**, 043808 (2005), doi:<https://doi.org/10.1103/PhysRevA.72.043808>
- [23] S. Floerchinger, M. Gärttner, T. Haas, and O. R. Stockdale, *Entropic entanglement criteria in phase space*, Phys. Rev. A **105**, 012409 (2022), doi:<https://doi.org/10.1103/PhysRevA.105.012409>
- [24] J. Gray, L. Banchi, A. Bayat and S. Bose, *Machine-Learning-Assisted Many-Body Entanglement Measurement*, Phys. Rev. Lett. **121**, 150503 (2018), doi:[10.1103/PhysRevLett.121.150503](https://doi.org/10.1103/PhysRevLett.121.150503)
- [25] A. Neven, J. Carrasco, V. Vitale *et al.*, *Symmetry-resolved entanglement detection using partial transpose moments*, npj Quantum Inf. **7**, 152 (2021), doi:<https://doi.org/10.1038/s41534-021-00487-y>
- [26] E. Majorana, *Atomi orientati in campo magnetico variabile*, Nuovo Cim **9**, 43 (1932), doi:[10.1007/BF02960953](https://doi.org/10.1007/BF02960953)
- [27] I. Bengtsson and K. Życzkowski, *Geometry of Quantum States : An Introduction to Quantum Entanglement*, 2nd ed. Cambridge University Press 2017, doi:[10.1017/9781139207010](https://doi.org/10.1017/9781139207010)
- [28] E. H. Lieb and J. P. Solovej, *Proof of an entropy conjecture for Bloch coherent spin states and its generalizations*, Acta Math. **212**, 379 (2014), doi:[10.1007/s11511-014-0113-6](https://doi.org/10.1007/s11511-014-0113-6)
- [29] T.-C. Wei and P. M. Goldbart, *Geometric measure of entanglement and applications to bipartite and multipartite quantum states*, Phys. Rev. A **68**, 042307 (2003), doi:[10.1103/PhysRevA.68.042307](https://doi.org/10.1103/PhysRevA.68.042307)
- [30] R. Hübener, M. Kleinmann, T.-C. Wei, C. González-Guillén and O. Gühne, *Geometric measure of entanglement for symmetric states*, Phys. Rev. A **80**, 032324 (2009), doi:[10.1103/PhysRevA.80.032324](https://doi.org/10.1103/PhysRevA.80.032324)
- [31] J. Martin, O. Giraud, P. A. Braun, D. Braun, and T. Bastin, Phys. Rev. A **81**, 062347 (2010), doi:[10.1103/PhysRevA.81.062347](https://doi.org/10.1103/PhysRevA.81.062347)
- [32] G. H. Hardy, J. E. Littlewood and G. Polya, *Inequalities*. 2nd ed. Cambridge University Press 1952, doi:[10.1017/S0025557200027455](https://doi.org/10.1017/S0025557200027455)
- [33] A function $f(q)$ is "little-o" of $g(q)$, i.e., $f(q) = o(g(q))$, as $q \rightarrow \infty$ if $\lim_{q \rightarrow \infty} f(q)/g(q) = 0$. A function $f(q)$ is "Big-o" of $g(q)$, i.e., $f(q) = \mathcal{O}(g(q))$, as $q \rightarrow \infty$ if $\exists M : |f(q)| \leq M g(q)$ in some neighborhood of ∞ .

- [34] M. Aulbach, D. Markham, and M. Murao, *The maximally entangled symmetric state in terms of the geometric measure*, New Journal of Physics **12**, 073025 (2010), doi:[10.1088/1367-2630/12/7/073025](https://doi.org/10.1088/1367-2630/12/7/073025)
- [35] C. Brezinski and M. Redivo-Zaglia, *The genesis and early developments of Aitken's process, Shanks transformation, the ϵ -algorithm, and related fixed point methods*, Numerical Algorithms **80**, 11 (2019), doi:<https://doi.org/10.1007/s11075-018-0567-2>
- [36] K. Fukushima, *Visual feature extraction by a multilayered network of analog threshold elements*, IEEE Transactions on Systems Science and Cybernetics **5**, 322 (1969), doi:[10.1109/TSSC.1969.300225](https://doi.org/10.1109/TSSC.1969.300225).
- [37] M. Innes, *Flux: Elegant Machine Learning with Julia*, Journal of Open Source Software **3**(25), 602 (2018), doi:[10.21105/joss.00602](https://doi.org/10.21105/joss.00602)
- [38] Danisch & Krumbiegel, *Makie.jl: Flexible high-performance data visualization for Julia*, Journal of Open Source Software, **6**(65), 3349 (2021), doi:[10.21105/joss.03349](https://doi.org/10.21105/joss.03349)
- [39] R. Pereira and J. Boneng, *The theory and applications of complex matrix scalings*, Special Matrices **2**, 68 (2014), doi:[10.2478/spma-2014-0007](https://doi.org/10.2478/spma-2014-0007)
- [40] T.-C. Wei and S. Severini, *Matrix permanent and quantum entanglement of permutation invariant states*, J. Math. Phys. **51**, 092203 (2010), doi:[10.1063/1.3464263](https://doi.org/10.1063/1.3464263)
- [41] T.-C. Wei, *Exchange symmetry and global entanglement and full separability*, Phys. Rev. A **81**, 054102 (2010), doi:<https://doi.org/10.1103/PhysRevA.81.054102>
- [42] A. Sugita, *Moments of generalized Husimi distributions and complexity of many-body quantum states*, J. Phys. A: Math. Gen. **36**, 9081 (2003), doi:[10.1088/0305-4470/36/34/310](https://doi.org/10.1088/0305-4470/36/34/310)
- [43] F. Bach, Approximating integrals with Laplace's method, <https://francisbach.com/laplace-method/>
- [44] A. Wehrl, *General properties of entropy*, Rev. Mod. Phys. **50**, 221 (1978), doi:<https://doi.org/10.1103/RevModPhys.50.221>
- [45] A. Wehrl, *On the relation between classical and quantum-mechanical entropy*, Rep. Math. Phys. **16**, 353 (1979), doi:[https://doi.org/10.1016/0034-4877\(79\)90070-3](https://doi.org/10.1016/0034-4877(79)90070-3)
- [46] G. Carleo, M. Troyer, *Solving the Quantum Many-Body Problem with Artificial Neural Networks*, Science **355**, 602 (2017), doi:<https://doi.org/10.48550/arXiv.1606.02318>